Available online at www.sciencedirect.com
SCIENCE DIRECT®
Journal of Solid State Chemistry 179 (2006) 161–168
JOURNAL OF SOLID STATE CHEMISTRY
www.elsevier.com/locate/jssc

Magnetic and vibrational properties and crystal structure of $Sr_{9.2}Co_{1.3}(PO_4)_7$ with disordered arrangements of some strontium, cobalt, and phosphate ions

Alexei A. Belik[a,*], Artem P. Malakho[b], Petro S. Salamakha[c,✠], Bogdan I. Lazoryak[d]

[a]*International Center for Young Scientists, National Institute for Materials Science, Namiki 1-1, Tsukuba, Ibaraki 305-0044, Japan*
[b]*Department of Materials Science, Moscow State University, 119922 Moscow, Russia*
[c]*Department of Chemistry, Institute of Nuclear Technology, P-2686 Sacavem, Portugal*
[d]*Department of Chemistry, Moscow State University, 119922 Moscow, Russia*

Received 28 June 2005; received in revised form 11 October 2005; accepted 16 October 2005
Available online 15 November 2005

Abstract

Solid solutions of $Sr_{9+x}Co_{1.5-x}(PO_4)_7$ were found in the compositional range of $0.05 \leqslant x \leqslant 0.30$. The structure of $Sr_{9.2}Co_{1.3}(PO_4)_7$ ($x = 0.2$) was determined from single crystal X-ray diffraction (space group $R\bar{3}m$ (No. 166); $Z = 3$; $a = 10.6100(5)$ Å and $c = 19.6960(5)$ Å; $V = 1920.17(14)$ Å^3; $\rho_{cal} = 4.014\,g\,cm^{-3}$; $\mu = 20.377\,mm^{-1}$) and refined to $R_1 = 0.0343$ and $wR_2 = 0.0633$ for 586 reflections with $I > 2\sigma(I)$. $Sr_{9.2}Co_{1.3}(PO_4)_7$ is structurally related to β-$Ca_3(PO_4)_2$ and $Sr_3(PO_4)_2$ and has disordered arrangements of some Sr^{2+}, Co^{2+}, and PO_4^{3-} ions. Sr^{2+} ions at a 9*e* site are statistically disordered among four positions near the center of symmetry. Co^{2+} and Sr^{2+} ions are split along the *c*-axis to occupy a 6*c* site that is 75% vacant. The $P1O_4$ tetrahedra are orientationally disordered. Sr^{2+} ions at an 8-fold coordinated 18*h* site, Co^{2+} ions at an octahedral 3*a* site, and the $P2O_4$ tetrahedra are ordered in the structure of $Sr_{9.2}Co_{1.3}(PO_4)_7$. Features of Raman spectra are discussed in relation to the crystallographic structure of $Sr_{9.2}Co_{1.3}(PO_4)_7$ and in comparison with Raman spectra of β-$Ca_3(PO_4)_2$-type and $Sr_3(PO_4)_2$-type compounds. $Sr_{9.2}Co_{1.3}(PO_4)_7$ is paramagnetic between 2 and 300 K with an effective magnetic moment of $4.98\mu_B$ per Co^{2+} ion.

Keywords: Strontium phosphate; Cobalt phosphate; Crystal structure; Single crystal; Raman spectroscopy; Magnetic susceptibility

1. Introduction

Tricalcium phosphate, $Ca_3(PO_4)_2$, and solid solutions including it as the end member have been extensively studied as (a) biomaterials [1,2], (b) luminescence materials [3], and (c) catalysts [4,5].

$Ca_3(PO_4)_2$ has several modifications. β-$Ca_3(PO_4)_2$ [6,7], which is the most studied in biomaterials, is stable above room temperature (RT) up to 1193 K [8–11]. β'-$Ca_3(PO_4)_2$ was observed above 1193 K up to 1408 K and this modification is not quenchable [8]. α-$Ca_3(PO_4)_2$ [12], thermodynamically stable between 1408 and 1703 K, is quenchable to RT [10]. α'-$Ca_3(PO_4)_2$ occurs above 1703 K [9,11]. α''-$Ca_3(PO_4)_2$ was observed by heating α-$Ca_3(PO_4)_2$ above 485 K [13]. Experimental evidence for low-temperature phase transitions was reported in the literature for the doped β-$Ca_3(PO_4)_2$, e.g., $Ca_{3-x}M_x(PO_4)_2$ (M = Cu and Sn) [14,15]. Temperatures of the phase transitions in $Ca_3(PO_4)_2$ strongly depend on the kind and amount of dopant [11,16].

In addition to the above-mentioned properties, compounds, which are isotypic with β-$Ca_3(PO_4)_2$ (space group $R3c$; $Z = 21$; $a = 10.439$ Å and $c = 37.375$ Å [6]) or have structures closely related to β-$Ca_3(PO_4)_2$, exhibit interesting dielectric properties and large second-harmonic generation (SHG). For example, $Ca_3(VO_4)_2$ [17] and $Sr_9M(VO_4)_7$ (M = Tm, Yb, and Lu) [18] show a ferroelectric phase transition and $Sr_9In(PO_4)_7$ and $Sr_9Fe(PO_4)_7$ [19] exhibit an antiferroelectric phase transition. $Ca_9Bi(VO_4)_7$ demonstrates a SHG signal of 140 times that of quartz [20].

*Corresponding author. Fax: +81 29 860 4706.
E-mail address: Alexei.BELIK@nims.go.jp (A.A. Belik).
✠Deceased

0022-4596/$ - see front matter © 2005 Elsevier Inc. All rights reserved.
doi:10.1016/j.jssc.2005.10.019

Even β'-$Ca_3(PO_4)_2$ is not quenchable to RT, it can be stabilized at RT by doping with Sr^{2+} ions, $Ca_{3-x}Sr_x(PO_4)_2$ with $13/7 \leqslant x \leqslant 16/7$ [8,16], e.g., $Ca_{5/7}Sr_{16/7}(PO_4)_2$. The crystal structure of $Ca_{5/7}Sr_{16/7}(PO_4)_2$ (space group $R\bar{3}m$; $Z = 10.5$; $a = 10.702$ Å and $c = 19.579$ Å [8]) is very similar to that of β-$Ca_3(PO_4)_2$; they differ in different degree of disordering of some structural elements. Ca^{2+} ions in $Ca_{5/7}Sr_{16/7}(PO_4)_2$ can be further replaced by (M^{2+}, Sr^{2+}) ions to give $Sr_{9+x}M_{1.5-x}(PO_4)_7$ (M = Mg, Fe, Ni, Cu, Zn, and Cd) that keeps the β'-$Ca_3(PO_4)_2$-type structure [16,21]. Note that high-temperature paraelectric phases of antiferroelectric $Sr_9In(PO_4)_7$ and $Sr_9Fe(PO_4)_7$ [19] and ferroelectric $Sr_9M(VO_4)_7$ (M = Tm, Yb, and Lu) [18] appeared to have the β'-$Ca_3(PO_4)_2$-type structure. The crystal structure of $Sr_{9.3}Ni_{1.2}(PO_4)_7$ was investigated using synchrotron X-ray and neutron powder diffraction data [21]. Some structural elements were found to be highly disordered in the structure of $Sr_{9.3}Ni_{1.2}(PO_4)_7$. Strontium–nickel phosphates have recently been investigated as catalysts [22]. Note that the structurally related $Ca_{3-x}Ni_x(PO_4)_2$ is an industrial catalyst [4].

The $Sr_{9+x}Co_{1.5-x}(PO_4)_7$ system has not been investigated yet. Because the structurally related $Ca_{3-x}Co_x(PO_4)_2$ system has catalytic activity [4], strontium–cobalt phosphates may also be interesting as catalysts. The problem related to the identification of active sites and components of catalysts requires detailed information about the crystal structure. For example, in $Ca_{3-x}Cu_x(PO_4)_2$, the catalytically active Cu^{2+} ions were found to locate at the $M4$ site [5].

In this work, we have investigated solid solutions with nominal compositions of $Sr_{9+x}Co_{1.5-x}(PO_4)_7$ ($0 \leqslant x \leqslant 0.5$) and obtained single crystals of $Sr_{9.2}Co_{1.3}(PO_4)_7$ ($x = 0.2$). For the first time, the crystal structure of the β'-$Ca_3(PO_4)_2$-type materials was determined from single-crystal X-ray diffraction data. Properties of $Sr_{9.2}Co_{1.3}(PO_4)_7$ were studied with magnetization measurements and Raman spectroscopy.

2. Experimental

Samples in the system $Sr_{9+x}Co_{1.5-x}(PO_4)_7$ with $x = 0$, 0.05, 0.1, 0.15, 0.2, 0.25, 0.3, 0.4, and 0.5 were synthesized by the solid-state method from stoichiometric mixtures of $SrCO_3$ (99.999%), Co_3O_4 (99.8%), and $NH_4H_2PO_4$ (99.999%). The mixtures were placed in alumina crucibles, heated in air while raising the temperature very slowly from RT to 873 K, reground, and then annealed at 1273 K for 120 h. They were reground every 30 h and finally quenched from 1273 K to RT. The samples were light-violet.

X-ray powder diffraction (XRD) data of the products were measured at RT on a SIEMENS D500 Bragg–Brentano-type powder diffractometer. The diffractometer was equipped with an incident-beam quartz monochromator to obtain Cu $K\alpha_1$ radiation ($\lambda = 1.5406$ Å) and a BRAUN position-sensitive detector. Si (NIST Standard Reference Material 640b) was used as an external standard material for diffraction angles. For phase identification, XRD data were collected in a 2θ range from 10° to 80° with a step interval of 0.02°. The resultant XRD data were analyzed by the Rietveld method with RIETAN-2000 [23]. We refined only lattice parameters of $Sr_{9+x}Co_{1.5-x}(PO_4)_7$, $Sr_3(PO_4)_2$ [24], and $Sr_2Co(PO_4)_2$ [25], fixing their structure parameters at those reported in the literature (or in this work). Mass fractions of constituent phases were calculated from the refined scale factors.

Polycrystalline single-phased sample $Sr_{9.2}Co_{1.3}(PO_4)_7$ ($x = 0.2$) was then annealed at 1523−1573 K for 50 h in a Pt crucible. Single crystals of $Sr_{9.2}Co_{1.3}(PO_4)_7$ with an average size of ca. 0.10 mm were found in the product obtained. XRD showed the crushed product to be monophasic. Single crystals of $Sr_{9.2}Co_{1.3}(PO_4)_7$ were polished in a special setup to form spherical particles. One crystal (among many twinned crystals) with radius of 0.069 mm was found to be suitable for X-ray diffraction experiments.

X-ray single-crystal diffraction data were obtained at RT on a four circle diffractometer (CAD-4) with graphite monochromatized Mo $K\alpha$ radiation ($\lambda = 0.71073$ Å). Lattice parameters were refined using 17 reflections. The intensities measured were corrected for absorption, polarization, and the Lorentz effects. Intensities of three reflections taken as standards were periodically recorded to check the stability of the data acquisition. Reflection conditions derived from the observed reflections were $-h + k + l = 3n$ (hexagonal axes, obverse setting). Further details of data collection and refinement results are listed in Table 1.

The structure of $Sr_{9.2}Co_{1.3}(PO_4)_7$ was successfully solved by the direct method in space group $R\bar{3}m$ and refined with a full-matrix least-squares program SHELXL-97 [26] (F^2 against all unique reflections) using atomic scattering factors for neutral atoms provided by this package. For disordered atoms, we refined isotropic atomic displacement parameters (U_{iso}). Anisotropic atomic displacement parameters, U_{ij}, were assigned to all sites with occupancy (g) of unity.

Table 2 lists the fractional atomic coordinates and U_{eq} and U_{iso} parameters. U_{ij} parameters are presented in Table 3. For $Sr_{9.2}Co_{1.3}(PO_4)_7$, we used site names similar to those of $Sr_{9.3}Ni_{1.2}(PO_4)_7$ [21].

SHG responses of the powder samples were measured in a reflection mode using 1064-nm radiation. A detailed description of the equipment and the methodology has been published elsewhere [8,21]. No SHG signals were observed in monophasic $Sr_{9+x}Co_{1.5-x}(PO_4)_7$ ($0.0 < x \leqslant 0.30$). Therefore, they can be considered as centrosymmetric in structure solution and refinement.

Magnetic susceptibilities, $\chi = M/H$, of $Sr_{9.2}Co_{1.3}(PO_4)_7$ were measured on a DC SQUID magnetometer (Quantum Design, MPMS XL) between 2 and 300 K in an applied field of 1000 Oe (1 Oe = $(10^3/4\pi)$ A m^{-1}) under both zero-field-cooled (ZFC) and field-cooled (FC) conditions. Isothermal magnetization curves of $Sr_{9.2}Co_{1.3}(PO_4)_7$ were recorded at 1.8 K between 0 and 70 kOe.

Specific heat, $C_p(T)$, of $Sr_{9.2}Co_{1.3}(PO_4)_7$ was measured between 1.9 and 30 K (on cooling) at zero magnetic field by a pulse relaxation method using a commercial calorimeter (Quantum Design PPMS).

Table 1
Parameters of single-crystal X-ray diffraction data collection and refinement for $Sr_{9.2}Co_{1.3}(PO_4)_7$

Formula	$Sr_{27.6}Co_{3.9}P_{21}O_{84}$
Temperature (K)	293(2)
Radiation, λ	Mo $K\alpha$, 0.71073 Å
Crystal habit	Spherical
Crystal radius (mm)	0.069
Crystal system	Trigonal
Space group	$R\bar{3}m$ (No. 166)
a (Å)	10.6100(5)
c (Å)	19.6960(5)
Volume (Å^3)	1920.17(14)
Z	1
Calculated density (g cm^{-3})	4.014
Linear absorption coefficient (mm^{-1})	20.377
$F(000)$	2140
Data range θ (°); h, k, l	2.45–34.94; $0 \leqslant h \leqslant 17$, $-8 \leqslant k \leqslant 0$, $-31 \leqslant l \leqslant 31$
Scan type	$\omega-\theta$
Total reflections; unique	3028; 1066
Number of reflections with $I > 2\sigma(I)$	586
Number of variables	58
Max./min. residual electron density (e Å^{-3})	2.23/−2.60
R_1[a]/wR_2[b] (for unique reflections)	0.1296/0.0819
R_1[a]; wR_2[b] ($I > 2\sigma(I)$)	0.0343; 0.0633
GooF (Goodness of fit)	1.024
Extinction coefficient	0.00089(6)

$w = 1/[\sigma^2(F_o^2) + (0.0194*P)^2 + 23.5058*P]$, where $P = (\mathrm{Max}(F_o^2, 0) + 2*F_c^2)/3$.
[a] $R_1 = \Sigma[|F_o| - |F_c|]/\Sigma|F_o|$ (with $|F_o|$ set to zero for negative F_o^2).
[b] $wR_2 = (\Sigma[w(F_o^2 - F_c^2)^2]/\Sigma w(F_o^2)^2)^{1/2}$.

Unpolarized Raman spectra of powder samples, $Sr_{9.2}Co_{1.3}(PO_4)_7$, $Sr_3(PO_4)_2$, and $Ca_9Fe(PO_4)_7$, were collected at RT with a micro-Raman spectrometer (Horiba Jobin-Yvon T64000) in backscattering geometry with a liquid-nitrogen-cooled CCD detector. Raman scattering was excited using an $Ar^+ - Kr^+$ laser at a wavelength of 514.5 nm. A 90 × long working distance objective was used to focus the laser beam onto a spot of about 2 μm in diameter. The laser power on the samples was about 2 mW.

3. Results and discussion

3.1. Structural properties

The samples with nominal compositions of $Sr_{9+x}Co_{1.5-x}(PO_4)_7$ ($0.05 \leqslant x \leqslant 0.30$) were monophasic whereas those with $x = 0.4$ and 0.5 contained $Sr_3(PO_4)_2$ and that with $x = 0$ contained $Sr_2Co(PO_4)_2$ as impurity phases. Fig. 1 displays the dependence of lattice parameters against the x value. These results indicate that solid solutions of $Sr_{9+x}Co_{1.5-x}(PO_4)_7$ are formed in a compositional range of $0.05 \leqslant x \leqslant 0.30$.

Single-crystal X-ray diffraction data confirmed the trigonal system for $Sr_{9.2}Co_{1.3}(PO_4)_7$ with lattice parameters of $a = 10.6100(5)$ Å and $c = 19.6960(5)$ Å (hexagonal setting) and the disordered structural model for $Sr_{9+x}M_{1.5-x}(PO_4)_7$ deduced from X-ray powder diffraction data of $Sr_{9.3}Ni_{1.2}(PO_4)_7$ [21]. That is, the single-crystal data revealed the orientational disorder of the $P1O_4$ tetrahedra and the positional disorder of Sr^{2+} ions at a 9e site ($M3$) and Co^{2+} and Sr^{2+} ions at a 6c site ($M4$).

Note that a special investigation was performed to find a possible superstructure in the c and a directions in $Sr_{9.2}Co_{1.3}(PO_4)_7$. However no superstructure reflections were detected. Electron diffraction and high-resolution electron microscopy studies also revealed no superstructure

Table 2
Fractional coordinates and atomic displacement parameters for $Sr_{9.2}Co_{1.3}(PO_4)_7$

Atom	Wyckoff position	g	x	y	z	U_{eq} or U_{iso}(Å^2)
Sr1	18h	1	0.18980(3)	$= -x$	0.53760(3)	0.01387(14)
Co5	3a	1	0	0	0	0.0105(4)
P1	3b	1	0	0	1/2	0.0429(14)
P2	18h	1	0.49222(8)	$= -x$	0.39760(7)	0.0127(3)
O21	18h	1	0.5345(3)	$= -x$	0.6758(2)	0.0275(11)
O22	36i	1	0.2651(3)	0.0122(3)	0.2345(2)	0.0194(6)
O24	18h	1	0.9100(2)	$= -x$	0.0678(2)	0.0164(8)
Sr31	18h	0.302(7)	−0.5130(3)	$= -x$	0.00871(11)	0.0116(6)
Sr32	18h	0.196(7)	−0.5351(4)	$= -x$	0.0144(2)	0.0120(11)
Sr4	6c	0.108(10)	0	0	0.3478(6)	0.013(2)
Co4	6c	0.144(12)	0	0	0.3645(11)	0.050(6)
O11	18h	0.333	−0.5903(11)	$= -x$	0.1193(10)	0.040(4)
O12	36i	0.167	−0.664(4)	0.788(3)	0.129(2)	0.061(9)

g is occupation factor.
$U_{eq} = (1/3)\ \Sigma_i\Sigma_j\ U_{ij}\ a_i^* a_j^*\ \boldsymbol{a}_i\ \boldsymbol{a}_j$.
U_{iso}: the isotropic Debye–Waller factor is computed as $\exp(-8\pi^2 U_{iso} \sin^2\theta/\lambda^2)$.

Table 3
Anisotropic atomic displacement parameters (Å^2) for $Sr_{9.2}Co_{1.3}(PO_4)_7$

Atom	U_{11}	U_{22}	U_{33}	U_{12}	U_{13}	U_{23}
Sr1	0.0127(2)	$=U_{11}$	0.0128(2)	0.0039(2)	−0.00108(11)	$=-U_{13}$
Co5	0.0101(5)	$=U_{11}$	0.0112(8)	$=0.5U_{11}$	0	0
P1	0.042(2)	$=U_{11}$	0.044(3)	$=0.5U_{11}$	0	0
P2	0.0146(5)	$=U_{11}$	0.0095(6)	0.0078(5)	−0.0002(3)	$=-U_{13}$
O21	0.036(2)	$=U_{11}$	0.010(2)	0.019(2)	−0.0026(10)	$=-U_{13}$
O22	0.0159(14)	0.0140(14)	0.0199(14)	0.0013(12)	−0.0010(11)	−0.0046(12)
O24	0.0127(14)	$=U_{11}$	0.022(2)	0.005(2)	0.0029(8)	$=-U_{13}$

The anisotropic Debye–Waller factor is computed as $\exp[-2\pi^2(h^2a^{*2}U_{11}+k^2b^{*2}U_{22}+l^2c^{*2}U_{33}+2hka^*b^*U_{12}+2hla^*c^*U_{13}+2klb^*c^*U_{23})]$.

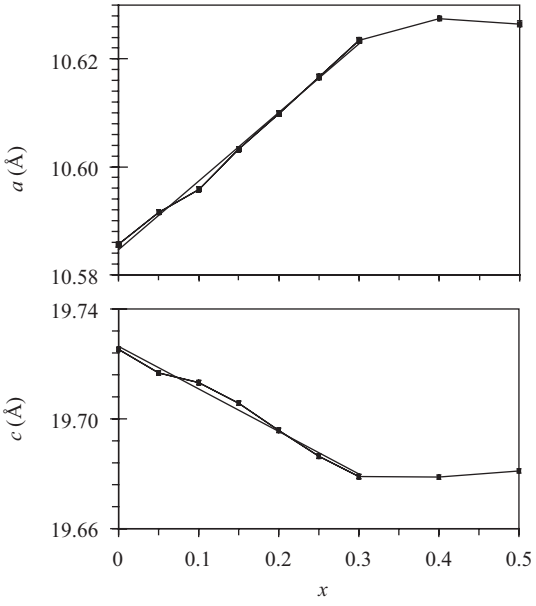

Fig. 1. Lattice parameters of solid solutions of $Sr_{9+x}Co_{1.5-x}(PO_4)_7$ ($0.0 \leqslant x \leqslant 0.5$) plotted against the x value.

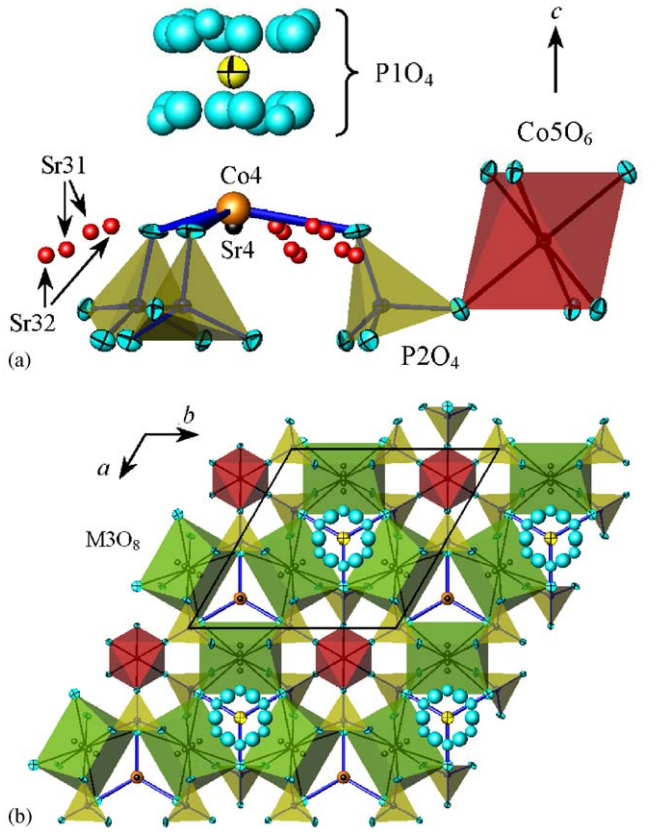

Fig. 2. (a) Disordered structural elements in $Sr_{9.2}Co_{1.3}(PO_4)_7$: the $P1O_4$ tetrahedron and the Sr31, Sr32, Sr4, and Co4 sites. The Co4–O21 bonds and ordered $P2O_4$ and $Co5O_6$ polyhedra are also shown. (b) Projection of the structure of $Sr_{9.2}Co_{1.3}(PO_4)_7$ along the c-axis. The $P2O_4$, $Co5O_6$, and $M3O_8$ polyhedra are given where the $M3$ is the ideal site (9e) for the Sr31 and Sr32 sites.

in the case of $Sr_{9.3}Ni_{1.2}(PO_4)_7$ [21]. Therefore the apparent static disorder cannot arise from lower true symmetry or missed supercell.

Sr^{2+} ions at the $M3$ site were found to be statistically distributed among four positions (two 18h sites: Sr31 and Sr32) near the center of symmetry (Fig. 2). We refined distribution of Sr^{2+} ions between the Sr31 and Sr32 sites without any constraints. The occupancy of the $M3$ site was unity within standard deviations. Sr^{2+} and Co^{2+} ions were found to be split along the (001) direction at the $M4$ site with coordinates (0, 0, 0.3478) for Sr4 and (0, 0, 0.3645) for Co4. Such relative shifts of the Sr4 and Co4 atoms are explained in terms of the large difference between the effective ionic radii of Co^{2+} and Sr^{2+} ions, 0.745 and 1.18 Å, respectively, for six-fold coordination [27]. Because the Sr4 and Co4 sites are separated only by 0.33 Å and these sites are partially occupied, the correlation between the g and U_{iso} parameters was observed. Therefore, the g and U_{iso} parameters of the Sr4 and Co4 sites were refined in different cycles (that is, not simultaneously), and g(Sr4) and g(Co4) were fixed on the last stage of our structure analysis. The refined composition was close to the nominal formula $Sr_{9.2}Co_{1.3}(PO_4)_7$ within standard deviations.

The large U_{eq}(P1) and U_{iso}(Co4) parameters may indicate that these atoms are located slightly off the three-fold rotational axis. But our attempts to move them from the 3b (for P1) and 6c (for Co4) sites failed because the x coordinate and U parameter are strongly correlated.

Ni^{2+} and Sr^{2+} ions in $Sr_{9.2}Ni_{1.3}(PO_4)_7$ [21] and Cu^{2+} and Sr^{2+} ions in $Sr_{9.1}Cu_{1.4}(PO_4)_7$ [28] were also found to be split at the $M4$ site. Ni^{2+} ions in $Sr_{9.2}Ni_{1.3}(PO_4)_7$ and Cu^{2+} ions in $Sr_{9.1}Cu_{1.4}(PO_4)_7$ were located slightly off the three-fold rotational axis.

U_{11}(O21) is larger by a factor of ca. 3 than U_{33}(O21). Because the O21 atoms are bonded to the highly disordered Sr31, Sr32, Co4, and Sr4 atoms, they are disordered to some extent as well. Such static positional disorder of O21 is absorbed into the U_{ij} parameters.

In $Sr_{9.2}Co_{1.3}(PO_4)_7$, oxygen atoms around the P1 site were localized at two sites from the difference Fourier synthesis, O11 (18*h*) and O12 (36*i*). The disordering of the four oxygen atoms covalently bonded to the P1 atom is rather complex. This fact is reflected in the large U_{iso}(O11) and U_{iso}(O12) parameters obtained using single-crystal X-ray diffraction data (as for $Sr_{9.2}Co_{1.3}(PO_4)_7$) or neutron powder diffraction data (as for $Sr_{9.3}Ni_{1.2}(PO_4)_7$ [21]).

$Sr_{9.2}Co_{1.3}(PO_4)_7$ (space group $R\bar{3}m$; $Z=3$; $a=10.6100$ Å and $c=19.6960$ Å) is structurally related to β-$Ca_3(PO_4)_2$ (space group $R3c$; $Z=21$; $a=10.439$ Å and $c=37.375$ Å) [6,7]) and α-$Sr_3(PO_4)_2$ (space group $R\bar{3}m$; $Z=3$; $a=5.3901$ Å and $c=19.785$ Å [24]). $Sr_{9.2}Co_{1.3}(PO_4)_7$ has a doubled a parameter in comparison with α-$Sr_3(PO_4)_2$ while β-$Ca_3(PO_4)_2$ has a doubled c parameter as compared with $Sr_{9.2}Co_{1.3}(PO_4)_7$. Structural relationships among β-$Ca_3(PO_4)_2$, α-$Sr_3(PO_4)_2$, and $Sr_{9+x}M_{1.5-x}(PO_4)_7$ were discussed in details in Ref. [8].

3.2. Magnetic properties of $Sr_{9.2}Co_{1.3}(PO_4)_7$

Fig. 3 presents plots of χ and χ^{-1} (ZFC curves) against temperature, T, for $Sr_{9.2}Co_{1.3}(PO_4)_7$. No noticeable difference was found between the curves measured under the ZFC and FC conditions. Between 100 and 300 K, the χ^{-1} vs T curve shows almost linear behavior and can be fitted by the simple Curie–Weiss equation:

$$\chi(T)=\frac{C}{T-\theta}, \quad (1)$$

where $C=3.101(8)\,cm^3\,K/Co\text{-}mol$ is the Curie constant and $\theta=-13.7(6)$ K is the Weiss constant. The negative Weiss constant implies antiferromagnetic interactions between Co^{2+} ions. The effective magnetic moment ($\mu_{eff}=(8C)^{1/2}$) was calculated to be $4.98\mu_B$ per a Co^{2+} ion. This value is typical for this ion which usually has a large orbital moment contribution in octahedral coordination [29,30]. Below 100 K, the deviation from the linear behavior was observed. Note that the χ^{-1} vs T data fit to Eq. (1) between 2 and 10 K resulted in $\mu_{eff}=4.04\mu_B$ per Co^{2+} ion and $\theta=-0.15$ K.

Fig. 4 depicts the isothermal magnetization curve, M vs H, at 1.8 K. At low magnetic fields below 10 kOe, the M vs H curve almost followed to the Brillouin function with $S=3/2$ and $g=2$. However above 10 kOe, the deviation from the Brillouin function was observed. The experimental M vs H curve saturated very slowly above about 30 kOe. Such

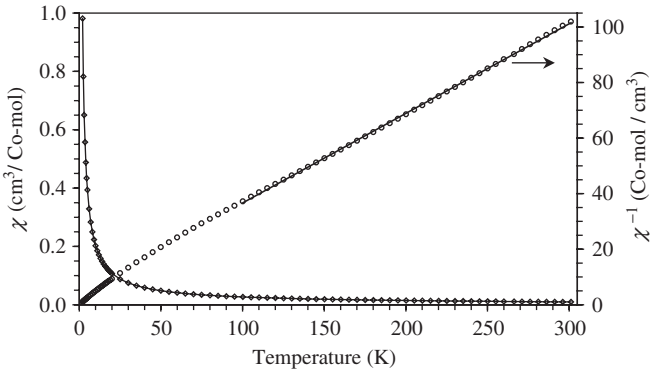

Fig. 3. The $\chi(T)$ (diamonds with line) and $\chi^{-1}(T)$ (circles) curves for $Sr_{9.2}Co_{1.3}(PO_4)_7$ measured in ZFC mode at 1000 Oe. The fit to Eq. (1) is given on the $\chi^{-1}(T)$ curve by the solid line.

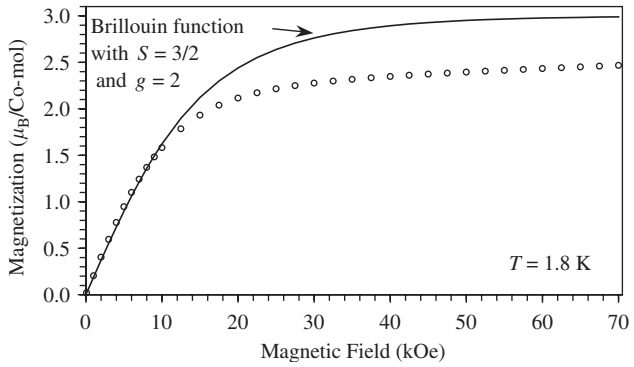

Fig. 4. The isothermal magnetization curve, M vs H, at $T=1.8$ K (circles). The solid line is the Brillouin function with $S=3/2$ and $g=2$.

behavior of the M vs H curve suggests the presence of interaction between Co^{2+} ions. The Co5 site occupied by Co^{2+} ions is surrounded by six $M4$ sites (Fig. 2). The $M4$ site is occupied by Co^{2+} with $g(Co)=0.15$. Therefore, a part of Co^{2+} ions at the $M5$ site may interact antiferromagnetically with Co^{2+} ions at the $M4$ site through super-superexchange interactions Co–O···O–Co, where the O···O is an edge of a PO_4 group. Super–superexchange interactions can be rather strong [31].

Temperature dependence of the specific heat divided by temperature, C_p/T vs T, of $Sr_{9.2}Co_{1.3}(PO_4)_7$ is given in Fig. 5 together with the C_p/T vs T curve of $Sr_{9.1}Cu_{1.4}(PO_4)_7$ for comparison [31]. Above about 8 K, the C_p/T vs T curves of $Sr_{9.2}Co_{1.3}(PO_4)_7$ and $Sr_{9.1}Cu_{1.4}(PO_4)_7$ coincide with each other. Therefore, it seems that there is only lattice contribution to the specific heat above 8 K. An increase of the C_p/T values was observed below 3 K for $Sr_{9.2}Co_{1.3}(PO_4)_7$. This increase is probably due to the Schottky-type contribution to the specific heat from Co^{2+} ions.

3.3. Vibrational properties of $Sr_{9.2}Co_{1.3}(PO_4)_7$

The internal vibrational modes of a free PO_4^{3-} tetrahedron with T_d symmetry are decomposed as A_1+E+2T_2

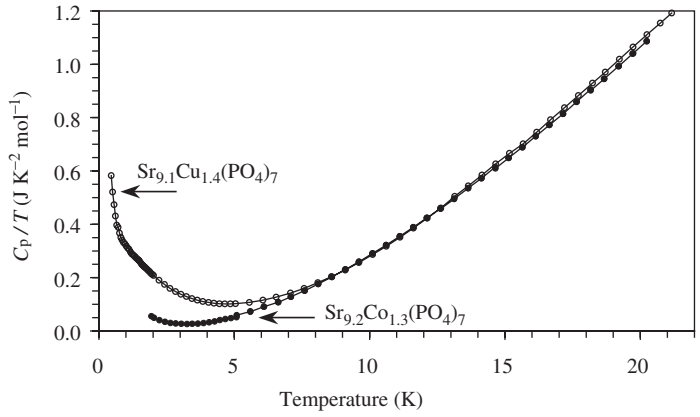

Fig. 5. The temperature dependence of C_p/T in $Sr_{9.2}Co_{1.3}(PO_4)_7$ and $Sr_{9.1}Cu_{1.4}(PO_4)_7$ given for comparison [31].

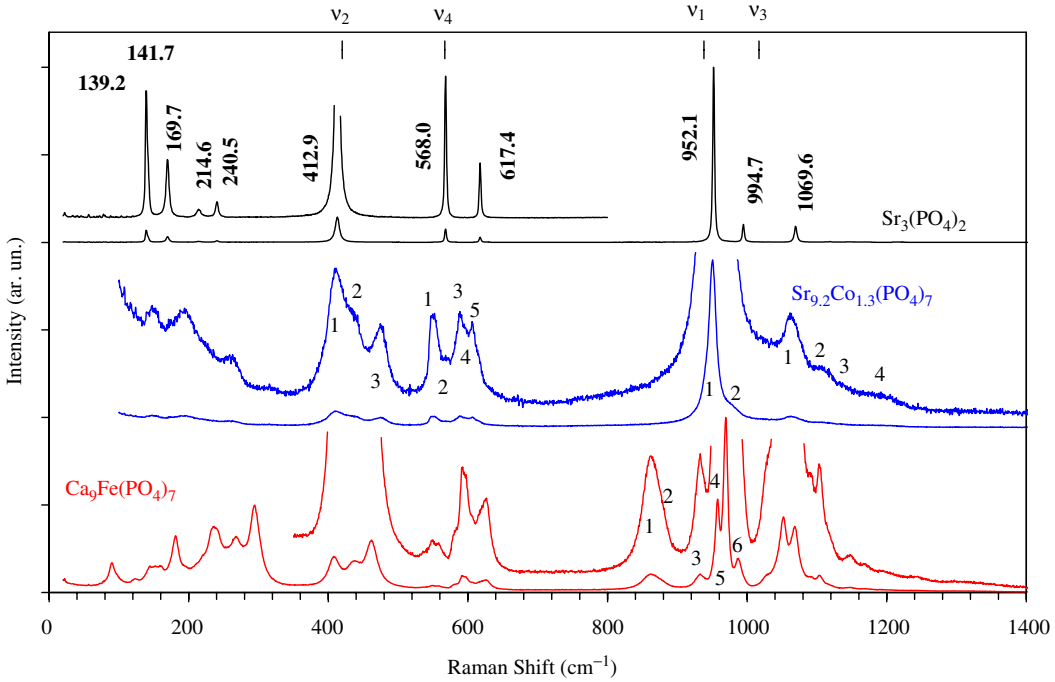

Fig. 6. Raman spectra of $Sr_3(PO_4)_2$, $Sr_{9.2}Co_{1.3}(PO_4)_7$, and $Ca_9Fe(PO_4)_7$. The tick marks on the top are the positions of the normal-mode frequencies of a free PO_4^{3-} tetrahedron (ν_2, ν_4, ν_1, and ν_3). Enlarge fragments of Raman spectra are also shown. For $Sr_3(PO_4)_2$, the frequencies of the observed bands are given. The numbers count the observed bands in each range corresponding to ν_2, ν_4, ν_1, and ν_3.

[32]. The mode with the A_1 symmetry type is the symmetric stretching mode (ν_1) of the P–O bonds. The modes with the E and T_2 symmetry types are bending O–P–O modes (ν_2 and ν_4, respectively). The second mode with the T_2 symmetry is the asymmetric stretching mode (ν_3). For a free PO_4^{3-} tetrahedron, $\nu_1 = 938\,cm^{-1}$, $\nu_2 = 420\,cm^{-1}$, $\nu_3 = 1017\,cm^{-1}$, and $\nu_4 = 567\,cm^{-1}$ [32].

Because $Sr_{9.2}Co_{1.3}(PO_4)_7$ has the structure which is intermediate between those of β-$Ca_3(PO_4)_2$ and α-$Sr_3(PO_4)_2$, it is interesting to compare vibrational properties of these three compounds. Vibrational properties of β'-$Ca_3(PO_4)_2$-type compounds have not been investigated yet. As a β-$Ca_3(PO_4)_2$-type compound, we selected $Ca_9Fe(PO_4)_7$ because there are no disordered structural elements in $Ca_9Fe(PO_4)_7$ [33] in comparison with β-$Ca_3(PO_4)_2$, where one site ($M4$) is half-occupied by Ca^{2+} ions [6].

The Raman spectra of α-$Sr_3(PO_4)_2$, $Sr_{9.2}Co_{1.3}(PO_4)_7$, and $Ca_9Fe(PO_4)_7$ are given in Fig. 6. The Raman bands are distributed in five distinct wavenumber ranges, 20–350, 350–530, 530–680, 800–990, and 990–1400 cm^{-1}. The first range corresponds to the lattice vibrations. The other ranges correspond to the internal modes ν_2, ν_4, ν_1, and ν_3 of a free PO_4^{3-} ion, respectively. The strongest band in all three compounds is derived from the ν_1 stretching mode of a free PO_4^{3-} tetrahedron.

Table 4
Factor group analysis of the internal modes of PO_4^{3-} tetrahedra in palmierite, $Sr_3(PO_4)_2$, and β-$Ca_3(PO_4)_2$-type compound, $Ca_9Fe(PO_4)_7$

Free PO_4^{3-} tetrahedron		$Sr_3(PO_4)_2$ D_{3d}^5 space group; $Z=1$	$Ca_9Fe(PO_4)_7$ C_{3v}^6 space group; $Z=2$	
Internal mode	T_d symmetry	2 PO_4^{3-} at C_{3v}	2 PO_4^{3-} at C_3	12 PO_4^{3-} at C_1
ν_1	A_1	$\boldsymbol{A_{1g}}+A_{2u}$	$\boldsymbol{A_1}+A_2$	$\boldsymbol{2A_1}+2A_2+\boldsymbol{4E}$
ν_2	E	$\boldsymbol{E_g}+E_u$	$2\boldsymbol{E}$	$\boldsymbol{4A_1}+4A_2+\boldsymbol{8E}$
ν_3	T_2	$\boldsymbol{A_{1g}}+A_{2u}+\boldsymbol{E_g}+E_u$	$\boldsymbol{A_1}+A_2+\boldsymbol{2E}$	$\boldsymbol{6A_1}+6A_2+\boldsymbol{12E}$
ν_4	T_2	$\boldsymbol{A_{1g}}+A_{2u}+\boldsymbol{E_g}+E_u$	$\boldsymbol{A_1}+A_2+\boldsymbol{2E}$	$\boldsymbol{6A_1}+6A_2+\boldsymbol{12E}$
Total	A_1+E+2T_2	$\boldsymbol{3A_{1g}}+\boldsymbol{3E_g}+3A_{2u}+3E_u$	$\boldsymbol{21A_1}+21A_2+\boldsymbol{42E}$	

Note. Modes marked by bold type are Raman active.

Table 5
Factor group analysis of the internal modes of PO_4^{3-} tetrahedra in $Sr_{9.2}Co_{1.3}(PO_4)_7$

Free PO_4^{3-} tetrahedron		$Sr_{9.2}Co_{1.3}(PO_4)_7$ D_{3d}^5 space group; $Z=1$	
Internal mode	T_d symmetry	6 PO_4^{3-} at C_s	"1 PO_4^{3-} at D_{3d}" 2 PO_4^{3-} at C_{3v}
ν_1	A_1	$\boldsymbol{A_{1g}}+\boldsymbol{E_g}+A_{2u}+E_u$	$\boldsymbol{A_{1g}}+A_{2u}$
ν_2	E	$\boldsymbol{A_{1g}}+\boldsymbol{2E_g}+A_{2u}+2E_u+A_{2g}+A_{1u}$	$\boldsymbol{E_g}+E_u$
ν_3	T_2	$\boldsymbol{2A_{1g}}+\boldsymbol{3E_g}+2A_{2u}+3E_u+A_{2g}+A_{1u}$	$\boldsymbol{A_{1g}}+A_{2u}+\boldsymbol{E_g}+E_u$
ν_4	T_2	$\boldsymbol{2A_{1g}}+\boldsymbol{3E_g}+2A_{2u}+3E_u+A_{2g}+A_{1u}$	$\boldsymbol{A_{1g}}+A_{2u}+\boldsymbol{E_g}+E_u$
Total	A_1+E+2T_2	$\boldsymbol{6A_{1g}}+\boldsymbol{9E_g}+6A_{2u}+9E_u+3A_{2g}+3A_{1u}$	

Note. Modes marked by bold type are Raman active.

The results of group analysis of the internal stretching and bending modes of PO_4^{3-} groups in the three compounds are given in Tables 4 and 5. Some comments should be given for the group analysis of $Sr_{9.2}Co_{1.3}(PO_4)_7$. The P1O_4 tetrahedron is disordered and the P1 atom is crystallographically located at the 3*b* site with the D_{3d} symmetry. However, D_{3d} is not a subgroup of T_d. Therefore the disordering should be artificially removed to perform group analysis. The simplest way to remove disordering is to consider the doubled unit cell in the *c* direction with the P1 atom at the C_{3v} site. The results of this analysis are given in Table 5. In reality, none of the oxygen atoms lay on the three-fold rotation axis while the P1 atom is located crystallographically on the three-fold rotation axis (Fig. 2a). Therefore, it is difficult to do the correct group analysis for the P1O_4 tetrahedron using its real orientation. Because of the highly disordered arrangement of P1O_4, we can assume that Raman bands due to vibration of P1O_4 should be rather weak and broad. Vibration of P2O_4 will be taken into account in the analysis of the Raman spectrum of $Sr_{9.2}Co_{1.3}(PO_4)_7$.

In α-$Sr_3(PO_4)_2$, six Raman modes are expected with only one mode derived from the ν_1 mode of a free PO_4^{3-} tetrahedron. All six modes were experimentally observed (Fig. 6). Note that in palmierite-like $Sr_3(VO_4)_2$ and $Ba_3(VO_4)_2$, only five bands were observed experimentally in the frequency ranges corresponding to the V–O stretching and O–V–O bending modes [34].

In $Ca_9Fe(PO_4)_7$, 63 Raman modes are expected with seven modes derived from the ν_1 mode of a free PO_4^{3-} tetrahedron. The number of Raman bands observed experimentally was much smaller than expected. Some bands were broadened because many bands overlap with each other. However, in the range of 800–990 cm^{-1} (ν_1), six bands were observed close to the predicted number. Note that in β-$Ca_3(PO_4)_2$, only four bands were found in this range using high-resolution measurements [32].

The Raman bands of $Sr_{9.2}Co_{1.3}(PO_4)_7$ are much broader compared with those of $Ca_9Fe(PO_4)_7$ and especially α-$Sr_3(PO_4)_2$. The broadening is due to the presence of many disordered structural elements in $Sr_{9.2}Co_{1.3}(PO_4)_7$. Fifteen Raman bands should be present in the wavenumber range corresponding to the P–O stretching and O–P–O bending modes with two modes derived from the ν_1 mode of a free PO_4^{3-} tetrahedron, three modes from the ν_2 mode, five modes from the ν_3 mode, and five modes from the ν_4 mode. Experimentally we observed 14 Raman bands (two bands for ν_1, three bands for ν_2, five bands for ν_4, and only four bands for ν_3) in good agreement with the prediction which considers only the P2O_4 tetrahedra.

4. Conclusion

In conclusion, we found solid solutions $Sr_{9+x}Co_{1.5-x}(PO_4)_7$ in the compositional range of $0.05 \leqslant x \leqslant 0.30$. Structure of $Sr_{9.2}Co_{1.3}(PO_4)_7$ was determined from single

crystal data. Some structural elements are highly disordered in $Sr_{9.2}Co_{1.3}(PO_4)_7$. Especially the complex orientational disorder of $P1O_4$ is difficult to describe adequately using spit atom models even by analyzing the single crystal data. $Sr_{9.2}Co_{1.3}(PO_4)_7$ was characterized with Raman spectroscopy and magnetization measurements.

Supporting information

Further details of the crystal structure investigation (cif-file and tables with bond lengths and angles) can be obtained from the Fachinformationszentrum Karlsruhe, 76344 Eggenstein-Leopoldshafen, Germany (fax: (49) 7247-808-666; e-mail: crysdata@fiz.karlsruhe.de) on quoting the depository number CSD 415800.

Acknowledgments

The authors thank A.V. Mironov of Moscow State University for the single-crystal X-ray diffraction experiment and S.Yu. Stefanovich of Moscow State University for the SHG study. This work was partially supported by the Russian Foundation for Basic Research (Grant 04-03-32417). ICYS is supported by Special Coordination Funds for Promoting Science and Technology from MEXT, Japan.

References

[1] (a) J.C. Elliott, Structure and Chemistry of the Apatites and Other Calcium Orthophosphates, Elsevier, Amsterdam, The Netherlands, 1994;
(b) K. De Groot, in: K. De Groot (Ed.), Bioceramics of Calcium Phosphate, CRC Press, Boca Raton, FL, 1983.
[2] A. Bigi, E. Foresti, M. Gandolfi, M. Gazzano, N. Roveri, J. Inorg. Biochem. 66 (1997) 259.
[3] H. Donker, W.M.A. Smit, G. Blasse, J. Electrochem. Soc. 136 (1989) 3130.
[4] A. Legrouri, S.S. Romdhane, J. Lenzi, M. Lenzi, G. Bonel, J. Mater. Sci. 31 (1996) 2469.
[5] A. Benarafa, M. Kacimi, G. Coudurier, M. Ziyad, Appl. Catal. A 196 (2000) 25.
[6] B. Dickens, L.W. Schroeder, W.E. Brown, J. Solid State Chem. 10 (1974) 232.
[7] M. Yashima, A. Sakai, T. Kamiyama, A. Hoshikawa, J. Solid State Chem. 175 (2003) 272.
[8] A.A. Belik, F. Izumi, S.Yu. Stefanovich, A.P. Malakho, B.I. Lazoryak, I.A. Leonidov, O.N. Leonidova, S.A. Davydov, Chem. Mater. 14 (2002) 3197.
[9] W. Fix, H. Heymann, R. Heinke, J. Am. Ceram. Soc. 52 (1969) 346.
[10] H. Monma, M. Goto, J. Ceram. Soc. Jpn. 91 (1983) 473.
[11] (a) E.R. Kreidler, F.A. Hummel, Inorg. Chem. 6 (1967) 524;
(b) E.R. Kreidler, F.A. Hummel, Inorg. Chem. 6 (1967) 884.
[12] M. Mathew, L.W. Schroeder, B. Dickens, W.E. Brown, Acta Crystallogr. Sec. B 33 (1977) 1325.
[13] L.J. Ruan, X.R. Wang, L.T. Li, Mater. Res. Bull. 31 (1996) 1207.
[14] A.L. Mackay, D.P. Sinha, J. Phys. Chem. Solids 28 (1967) 1337.
[15] S.S. Romdhane, G. Bonel, G. Bacquet, Mater. Res. Bull. 18 (1983) 559.
[16] J.F. Sarver, M.V. Hoffman, F.A. Hummel, J. Electrochem. Soc. 108 (1961) 1103.
[17] A.M. Glass, S.C. Abrahams, A.A. Ballmann, G. Loiacono, Ferroelectrics 17 (1978) 579.
[18] (a) A.A. Belik, M. Takano, M.V. Boguslavsky, S.Yu. Stefanovich, B.I. Lazoryak, Chem. Mater. 17 (2005) 122;
(b) A.A. Belik, M. Azuma, M. Takano, Solid State Ionics 172 (2004) 533.
[19] (a) S.Yu. Stefanovich, A.A. Belik, M. Azuma, M. Takano, O.V. Baryshnikova, V.A. Morozov, B.I. Lazoryak, O.I. Lebedev, G. Van Tendeloo, Phys. Rev. B 70 (2004) 172103;
(b) A.A. Belik, F. Izumi, M. Azuma, T. Kamiyamam, K. Oikawa, K.V. Pokholok, B.I. Lazoryak, M. Takano, Chem. Mater 17 (2005) 5455.
[20] (a) B.I. Lazoryak, O.V. Baryshnikova, S.Yu. Stefanovich, A.P. Malakho, V.A. Morozov, A.A. Belik, I.A. Leonidov, O.N. Leonidova, G. Van Tendeloo, Chem. Mater. 15 (2003) 3003;
(b) J.S.O. Evans, J. Huang, A.W. Sleight, J. Solid State Chem. 157 (2001) 255.
[21] A.A. Belik, F. Izumi, T. Ikeda, V.A. Morozov, R.A. Dilanian, S. Torii, E.M. Kopnin, O.I. Lebedev, G. Van Tendeloo, B.I. Lazoryak, Chem. Mater. 14 (2002) 4464.
[22] S.J. Lee, J.H. Jun, S.-H. Lee, K.J. Yoon, T.H. Lim, S.-W. Nam, S.-A. Hong, Appl. Catal. A 230 (2002) 61.
[23] F. Izumi, T. Ikeda, Mater. Sci. Forum 321–324 (2000) 198.
[24] K. Sugiyama, M. Tokonami, Mineral. J. 15 (1990) 141.
[25] A.A. Belik, B.I. Lazoryak, T.P. Terekhina, S.N. Polyakov, Russ. J. Inorg. Chem. 46 (2001) 1312.
[26] G.M. Sheldrick, SHELXL-97, Program for Crystal Structure Refinement, University of Gottingen, Germany, 1997.
[27] R.D. Shannon, Acta Crystallogr. Sec. A 32 (1976) 751.
[28] A.A. Belik, A.P. Malakho, B.I. Lazoryak, S.S. Khasanov, J. Solid State Chem. 163 (2002) 121.
[29] C. Kittel, Introduction to Solid State Physics, sixth ed, Wiley, New York, 1986, p. 406.
[30] Z. He, D. Fu, T. Kyomen, T. Taniyama, M. Itoh, Chem. Mater. 17 (2005) 2924.
[31] A.A. Belik, M. Azuma, M. Takano, J. Magn. Magn. Mater. 272–276 (2004) 937.
[32] P.N. de Aza, C. Santos, A. Pazo, S. de Aza, R. Cusco, L. Artus, Chem. Mater. 9 (1997) 912.
[33] B.I. Lazoryak, V.A. Morozov, A.A. Belik, S.S. Khasanov, V.Sh. Shekhtman, J. Solid State Chem. 122 (1996) 15.
[34] A. Grzechnik, P.F. McMillan, J. Solid State Chem. 132 (1997) 156.